Fractals in Society and Nature

Pratham Patil, Roger Felix Alcantara-Tangonan,
Vanessa Montoya,Wing Yan Jane Yip

30 March 2024

1 Introduction

Fractals are geometric shapes that contain some repetition or self-similarity at smaller scales (Strogatz, 2015). The prevalence of fractals is widespread. From being purely mathematical objects to describing how blood vessels are distributed in the lungs, fractals appear in many areas of society and nature. The majority of the theory is presented in Strogatz, 2015 as part of the course structure, but in the interest of being prudent, any relevant theory required to understand an application or example is self-contained within its respective section.

In this report, we will first present fractals in the context of image compression and medicine. These two topics will encompass how fractals can be applied to approach problems in industry. Next, we will investigate fractals arising in city structures and condensed matter physics (Hofstadter's butterfly). These two topics will provide examples of how fractals arise in nature and allow us to present some calculation-based information.

2 Applications of Fractals

2.1 Fractal Image Compression

2.1.1 Introduction to Image Compression

JPEG is the most widely used image encoding format where a discrete cosine transform (DCT) compression is applied. According to the JPEG compression process explained in the textbook by Mazet, 2020, DCT is similar to Discrete Fourier Transform (DFT), and a range of 2D cosine frequencies are obtained from the original image. The compression is done through the filtering of high frequencies which the human eyes are less sensitive to. As a result, the JPEG image obtained through the inverse DFT after the compression is defined as lossy, due to the process being irreversible. While JPEG is an efficient image compression format, there is a need to explore other means of image compression, in order to achieve a large compression while retaining a high level of detail. Other means of algorithmic encoding for images include fractals and wavelet transformations. Wavelet transformation filters out high-detail data, while fractal compression attempts to encode information in a compact way (Welstead, 1999).

The pioneer in the development of fractal image compression was led by Michael Barnsley in 1984, where iteration function systems (IFS) were introduced as a means to reconstruct fractals globally (Barnsley & Demko, 1985). Due to the limited scope of our study, the rich theory behind Barnsley's IFS will not be discussed nor proven here. Consider the following example of a fern fractal binary image constructed through an iterated function system. IFS by itself is ineffective at encoding normal pictures, due to IFS are only able to encode globally self-similar objects.

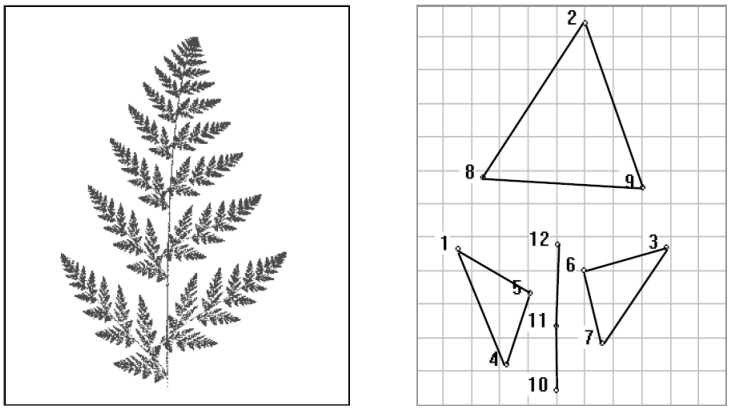

Figure 1: Figure a) is an image of a fern constructed through IFS. Notice how each of the leaves are similar to the branches and to the fern itself. Figure b) represents the 24 floating point values required, together with four transformations mapping the fern onto the four sub-images in Figure b) for the reconstruction of Fig a).(Welstead, 1999).

2.1.2 Partitioned Iterated Function Systems

The actual image encoding applied to real images is called partitioned iterated function systems (PIFS). Affine transformations are applied to the gray scale image where translation, rotation, and contractions are possible. $\widetilde{w}_i$ represents the spatial mapping between the subdomain $D_i \subset \boldsymbol{I}^2$ unit square, and the range R_i from the $\widetilde{w}_i$ operation, such that $\widetilde{w}_i(D_i) = R_i$. The affine transformation $\widetilde{w}_i$ has to be invertible since the encoding and decoding of the image has to be allowed. For a gray scale image, additional information such as the contrast and brightness of the image are included in the operation. For an example of a partition on the range cells of the image, Fig.3 shows an example of a real image, where the size of range cells are adaptive. Details of the image can be partitioned into smaller range cells to preserve information.

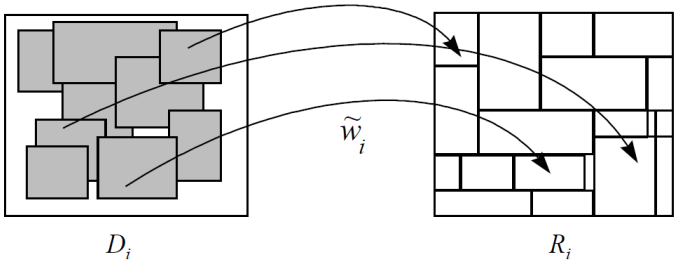

Figure 2: This is a representation of the PIFS. The $\widetilde{w}_i$ transformation maps D_i to the range R_i. While the domains may overlap, the range has to fit the unit square (Welstead, 1999).

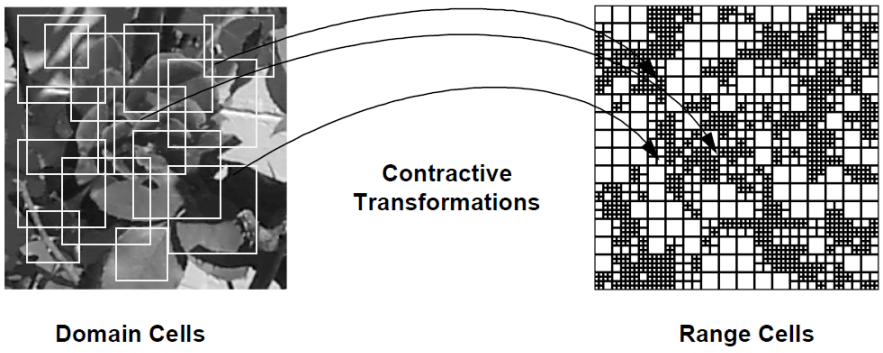

Figure 3: An example of fractal encoding attempt in computing the contractive transformation W that maps the domain cells to the range cells(Welstead, 1999).

Next, the most important part of fractal image compression is the contraction mapping. According to the definition in Barnsley, 1993, a function $f : \boldsymbol{X} \to \boldsymbol{X}$ mapping on a complete metric space $(\boldsymbol{X}, d)$ is said to be contractive if f posses exactly one fixed point $x_f \in \boldsymbol{X}$, and for any point $x \in \boldsymbol{X}$, the sequence of functions $\{f^{\circ n}(x) : n = 0, 1, 2, ...\}$ converges to x_f. That is

$$\lim_{n\to\infty} f^{\circ n}(x) = x_f, \text{ for each } x \in \boldsymbol{X} \tag{1}$$

In other words, for a contractive W that maps from any starting image, through iteration of W, the transformation of the starting image will eventually converge on the fixed point image, regardless of the initial conditions (Welstead, 1999). Fig.4 is an excellent example in recovering the image from two different starting image. Fractal image compression is achieved through the contractive transformation W storing all the information required to recover the image from any starting point. When the storage space required for W is less than the space required to store the image, image compression is a success.

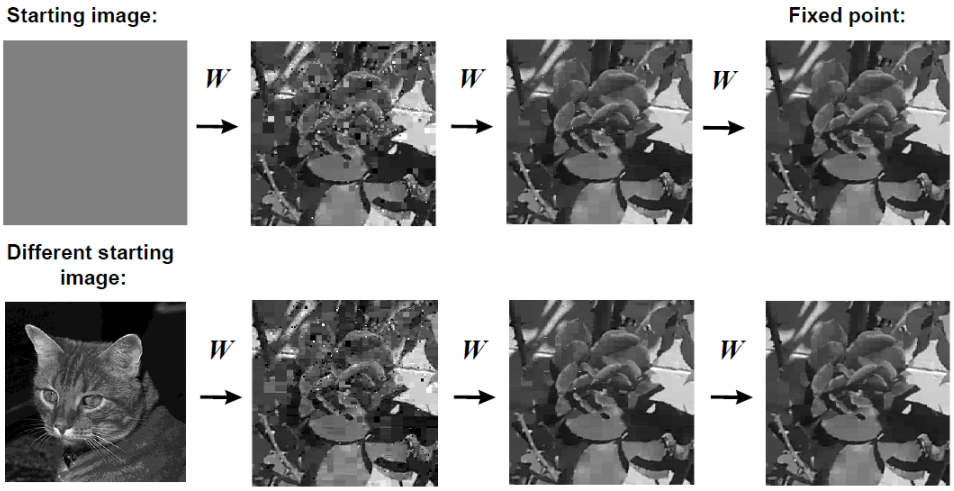

Figure 4: An example of contractive transformation W applied iteratively to two different starting images, and recovering the same image (Welstead, 1999).

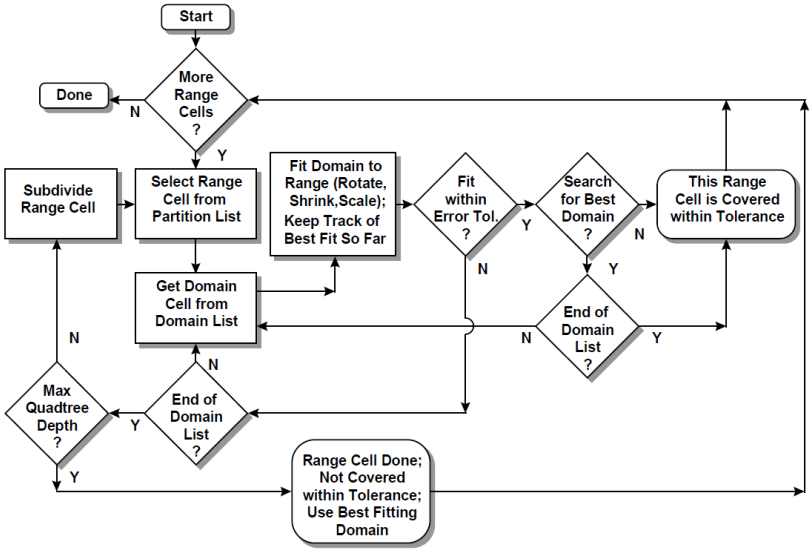

Figure 5: An example of a work flow of a fractal image compression software. The most computationally intensive step is the fitting of the domain and corresponding transformation that best fit the range cells (Welstead, 1999).

2.1.3 Results of Fast Fractal Image Compression

Modern day research on fractal image compression aims to shorten the computation time required to fit the contractive transformation with the domain and range cells. In this example, the group explored a faster method in retrieving the transformation for the range cells. Their fractal compression quality was comparable to the traditional compression methods such as JPEG (Commuri et al., 2020). In Fig. 6, the results from their research shows that while traditional compression methods may out perform partition iteration function systems at high compression ratios, the PIFS fractal compression maintains a stable and similar PSNR compared to traditional methods at moderate compression. Traditional methods out perform fractals compression due to the image filter being applied to each individual block of partitioned images, in formats such as JPEG, and compression artefacts are independent to each block.

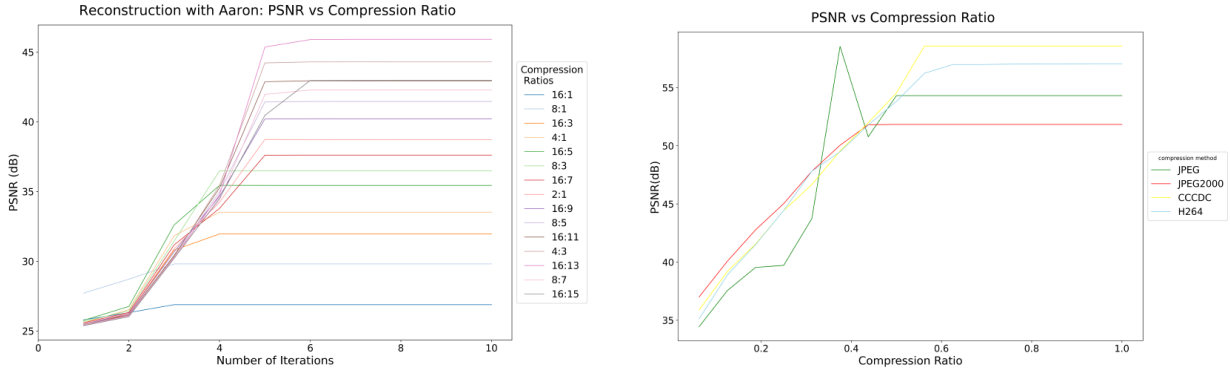

Figure 6: The peak signal to noise ratio (PSNR) obtained through iteration of the transformation in fractal compression on the left, compared to the PSNR of traditional compression methods(Commuri et al., 2020).

To conclude, while there are limitations to fractal image compression method in terms of the quality and computational time, it is an interesting method for encoding information. From the rich background in the development of iterated function systems to the application of fractals, there is a lot left to be explored.

2.2 Fractals and Medicine

Fractal dimension analysis has shown great potential in detecting different stages of cancer using transmission optical microscopy. Fractal dimension is a measure of self-similarity in a structure and is a powerful physical parameter for the characterization of structural properties of many partially filled disordered materials. Biological tissues are fractal and reports show a change in self-similarity associated with the progress of cancer, resulting in changes in their fractal dimensions (Elkington et al., 2022). The fractal dimension of the tissue structure is directly proportional to its mass density, which increases with the rapid reproduction of cancerous cells (Elkington et al., 2022). This makes fractal dimension analysis a potential technique for the detection of different stages of cancer using transmission optical microscopy.

The technique involves measuring the fractal dimension of different cancer stages using tissue micro array (TMA) samples containing pancreatic, breast, colon, and prostate cancers. The TMA samples are tissue cores of diameter 1.5mm and thickness 5μm. They are enveloped in paraffin wax to increase the shelf life of the samples. The cores are aligned in rows on a glass slide, each glass slide containing various stages of the cancer in question and a cancer-free control sample. The technique uses transmission optical microscopy of each thin tissue sample. This produces an intensity distribution pattern proportional to its refractive index pattern, representing the sample's mass density distribution. The refractive index is a direct result of mass density, where larger mass densities correspond to a larger refractive index. The result is a bright field image with information on the mass density. The bright field image is converted to a binary image using the computer program J image. The fractal dimension of each binary image is calculated using the box-counting method. The binary image is overlaid with a grid of squares with side length ϵ. The relationship between the $N(\epsilon)$ number of squares of side length ϵ needed to cover the fractal is:

$$d = \frac{\ln N(\epsilon)}{\ln \frac{1}{\epsilon}}$$

where d is the fractal dimension. The algorithm used in this study calculates the average fractal dimension by plotting $\ln N(\epsilon)$ vs. $\ln \frac{1}{\epsilon}$. The slope of this graph is the average fractal dimension. Figures 7,8,9,10 show the results of the study.

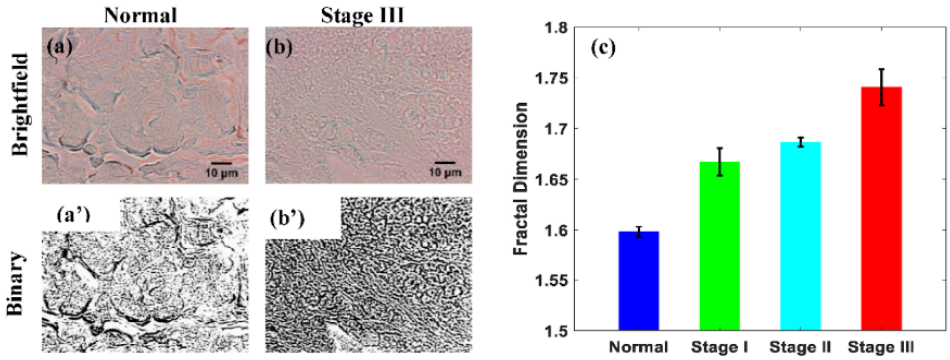

Figure 7: Pancreatic Cancer Fractal dimension analysis. Figures (a) and (a') show the Bright field and Binary image of normal pancreatic tissue. Figures (b) and (b') show the bright field and binary image of stage III Pancreatic cancer. The dark areas of the binary images (a') and (b') represent areas of high mass density. Notice how the binary image of stage III cancer in (b') has a darker tone and smaller compact fractal structures compared to the normal tissue shown in (a'). Figure c) shows the average fractal dimension of the samples in each stage of Pancreatic cancer. The actual fractal dimensions for each sample are calculated to be 1.5984 for the normal, 1.6673 for stage I, 1.6866 for stage II, and 1.7407 for stage III. The percent difference between the normal and stage I sample is 4%, between normal and stage II is 6%, and between normal and stage III is 9% (Elkington et al., 2022)

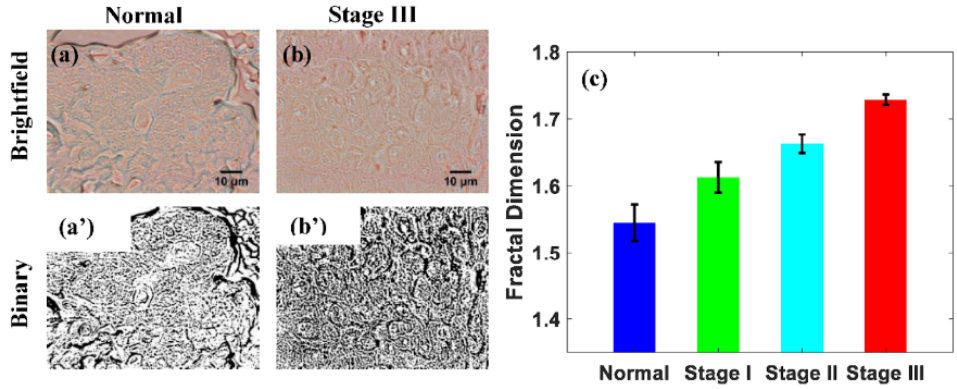

Figure 8: Breast Cancer Fractal dimension analysis. Figures (a) and (a') show the Bright field and Binary image of normal pancreatic tissue. Figures (b) and (b') show the bright field and binary image of stage III Pancreatic cancer. The dark areas of the binary images (a') and (b') represent areas of high mass density. Notice how the binary image of stage III cancer in (b') has a darker tone and smaller compact fractal structures compared to the normal tissue shown in (a'). Figure c) shows the average fractal dimension of the samples in each stage of Breast cancer. The actual fractal dimensions of the breast tissue samples are 1.5448 for the normal, 1.6126 for stage I, 1.6631 for stage II, and 1.7284 for stage III cancer The results show the fractal dimension of cancer stage I increases by 4%, stage II by 7%, and stage III by 12% with respect to the normal (Elkington et al., 2022).

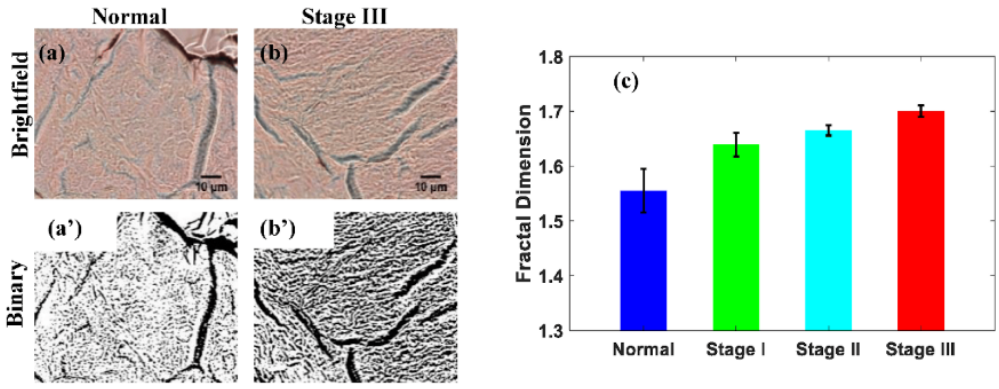

Figure 9: Colon Cancer Fractal dimension analysis. Figures (a) and (a') show the Bright field and Binary image of normal Colon tissue. Figures (b) and (b') show the bright field and binary image of stage III Colon cancer. The dark areas of the binary images (a') and (b') represent areas of high mass density. Notice how the binary image of stage III cancer in (b') has a darker tone and smaller compact fractal structures compared to the normal tissue shown in (a').Figure c) shows the average fractal dimension of the samples in each stage of Colon cancer. The actual fractal dimension values for each sample are 1.5551 for the normal, 1.6393 for stage I, 1.6652 for stage II, and 1.7004 for stage III. The results show the fractal dimension of cancer stage I increases by 5%, stage II by 7%, and stage III by 9% compared to the normal fractal dimension(Elkington et al., 2022).

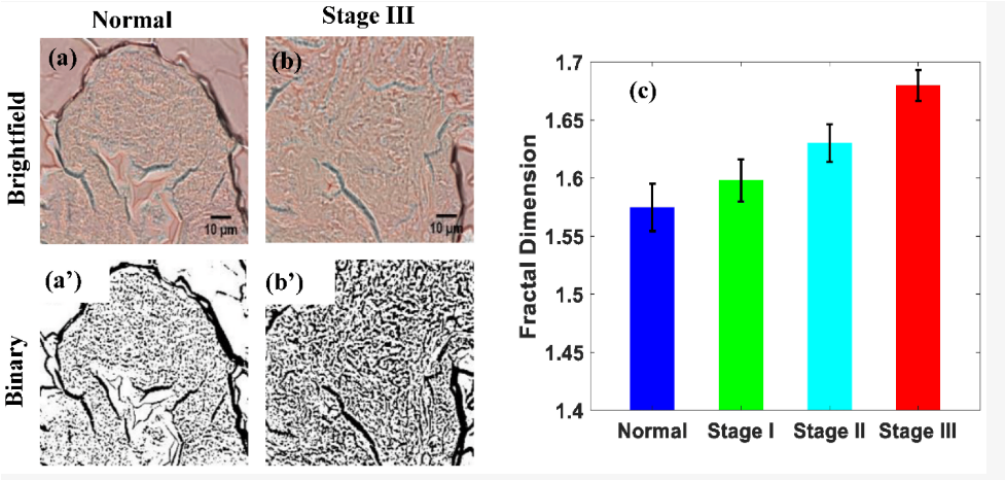

Figure 10: Prostate Cancer Fractal dimension analysis. Figures (a) and (a') show the Bright field and Binary image of normal Colon tissue. Figures (b) and (b') show the bright field and binary image of stage III Colon cancer. The dark areas of the binary images (a') and (b') represent areas of high mass density. Notice how the binary image of stage III cancer in (b') has a darker tone and smaller compact fractal structures compared to the normal tissue shown in (a'). Figure c) shows the average fractal dimension of the samples in each stage of Prostate cancer. The actual fractal dimension values for each sample are 1.5737 for the normal, 1.5981 for stage I, 1.6302 for stage II, and 1.6798 for stage III. The results show the fractal dimension of cancer stage I increases by 2%, stage II increases by 4%, and stage III by 7% with respect to the normal (Elkington et al., 2022)

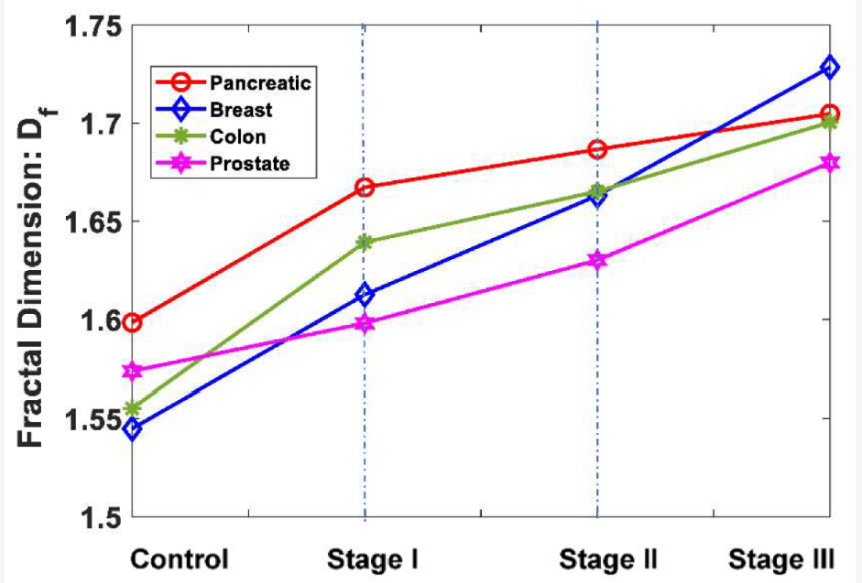

Figure 11: The average fractal dimension for the stages of Pancreatic, Breast, Colon, and Prostate cancer is shown. All Cancers increase in fractal dimension as they progress.

The fractal dimension method correctly differentiates cancer stages in progressive cancer, raising possibilities for a physics-based accurate diagnosis method for cancer detection. Cancer diagnosis has been a challenging field due to the difficulty in detecting cancers that are in their early stages. Current methods require either expensive chemical dyes and equipment or careful observation by a pathologist, making it time-consuming, inefficient, and susceptible to human error. Fractal dimension analysis of microscopic tissue images could automate the process, making cancer testing more accessible to the public and increasing the chances of early cancer diagnosis.

In conclusion, the potential of fractal dimension analysis to differentiate the fractal dimensions of healthy tissue and cancerous tissue is a promising and exciting area of research that could have a significant impact on the field of medicine. The technique has shown great potential in detecting different stages of cancer using transmission optical microscopy and could lead to earlier detection, better survival rates, and faster recovery times for those prone to cancer.

3 Examples of Fractals in Society and Nature

3.1 Fractal Cities

Fractal cities. Fractal cities are those that tend to develop over time in fractal patterns. The pattern that emerges as a sizable fractal city absorbs its surrounding towns and villages resembles a self-similar structure. Although it initially appears random, this dynamic network may end up being more effective than contemporary "pre-planned" cities. Figure 12 shows a southern Ohio city's development in the 19th century, showing fractal-like patterns.

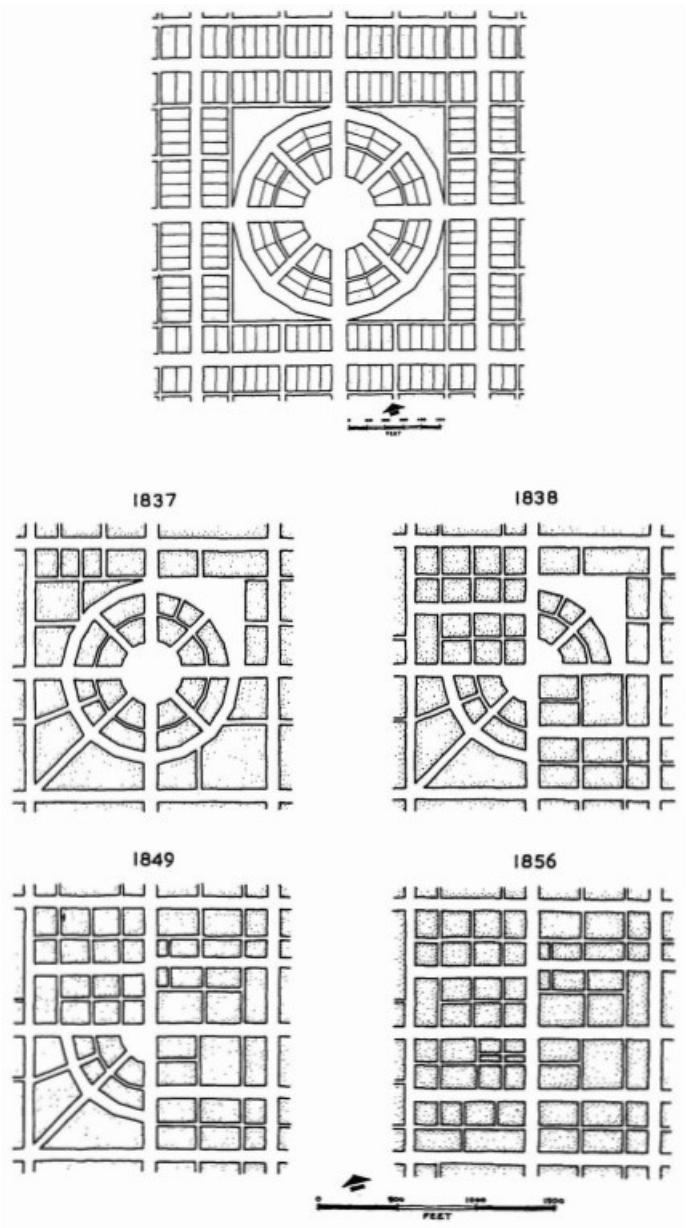

Figure 12: The squaring of Circleville 1810-1856 (Batty & Longley, 1994).

The following images are further examples to get a sense of Fractal City Geometry.

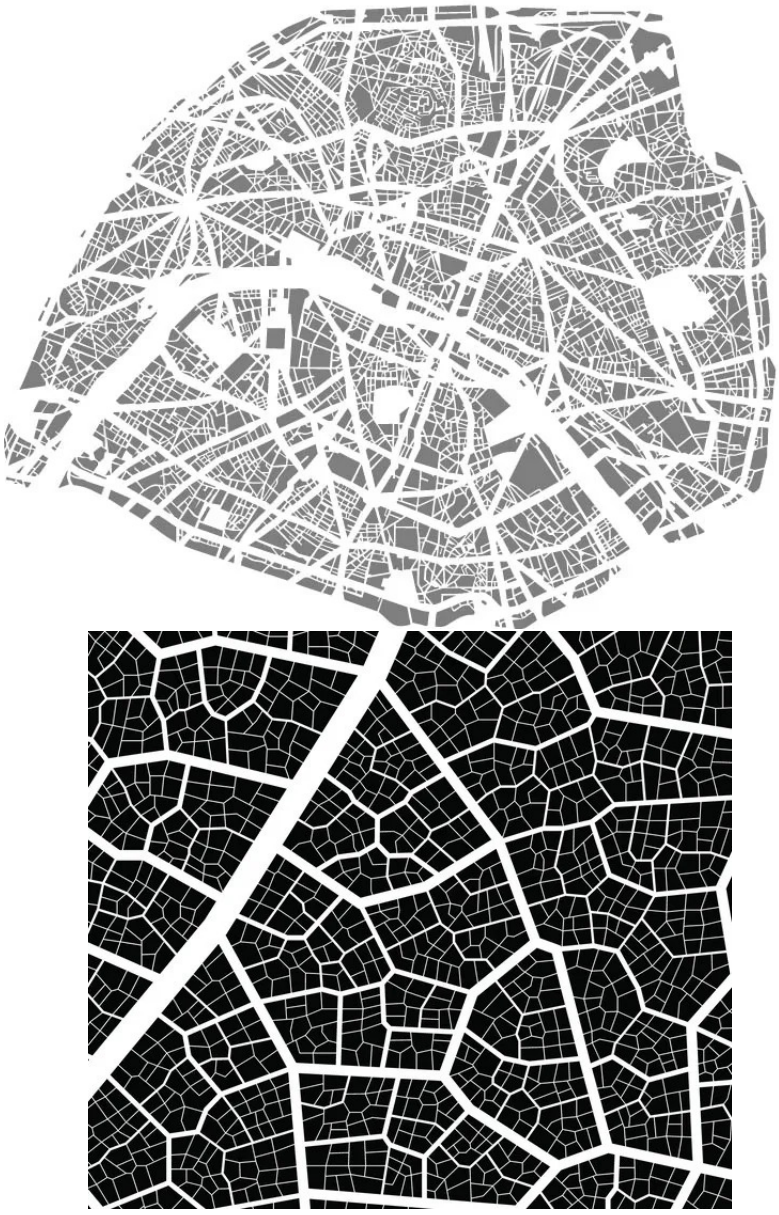

Figure 13: Examples of City Fractals (Whitney, 2018)

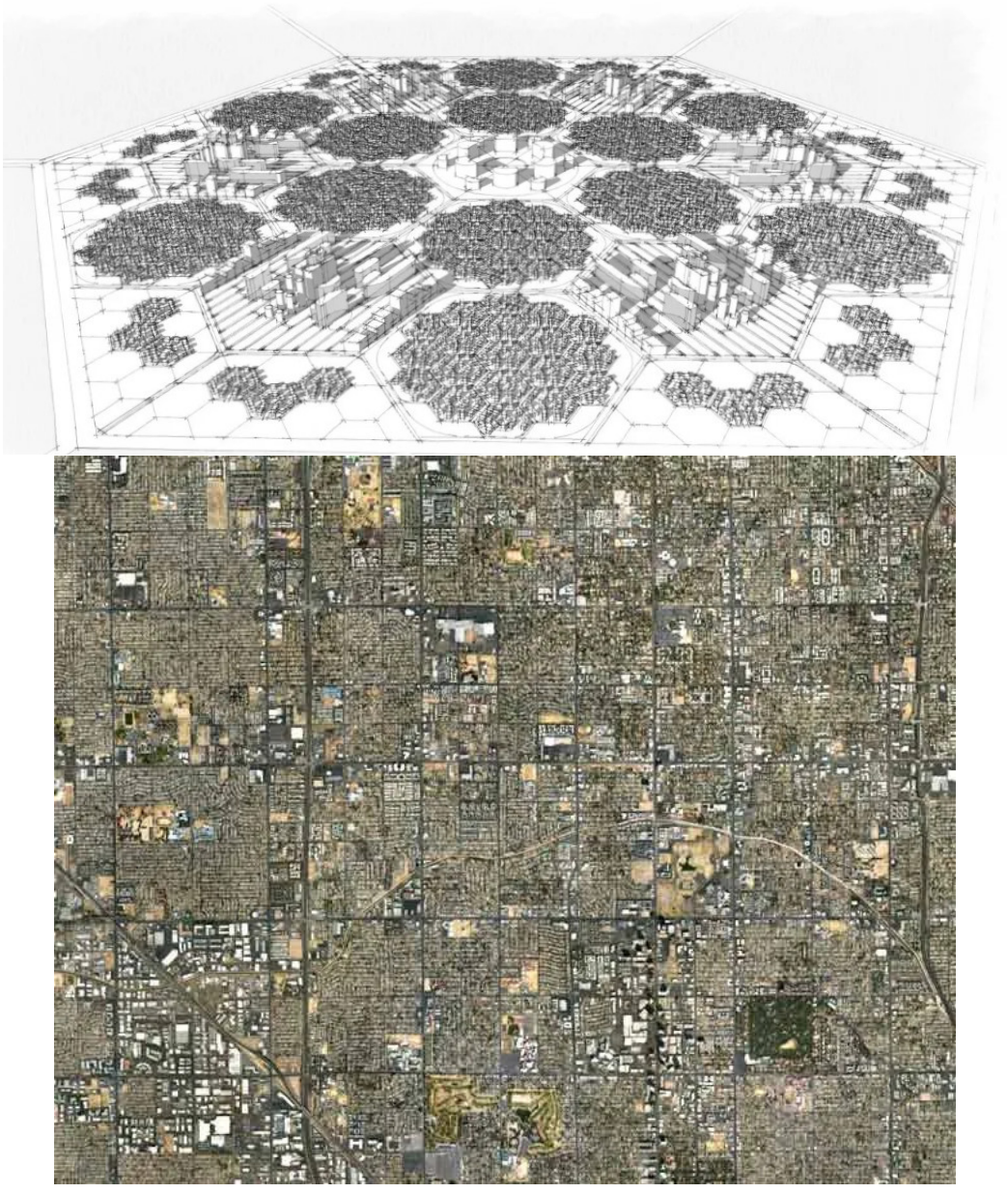

Figure 14: Examples of City Fractals (Whitney, 2018)

Most cities (˜95%) "organically" display fractal features, this is the main consensus (Batty & Longley, 1994). However, few examples do have features that have been controlled or planned before. Exact self-similarity is also not often seen. There are instead self-affine fractals, which indicates that scaling ratios can vary. This type of fractal would be self-similar in that it would include copies of the object at every size, but these copies would be somehow altered from the original initiator. Next, Figure 15 shows the three categories of fractals often found in the city space. A comparison between (b) and (c) demonstrates that the network is a hierarchy and vice versa.

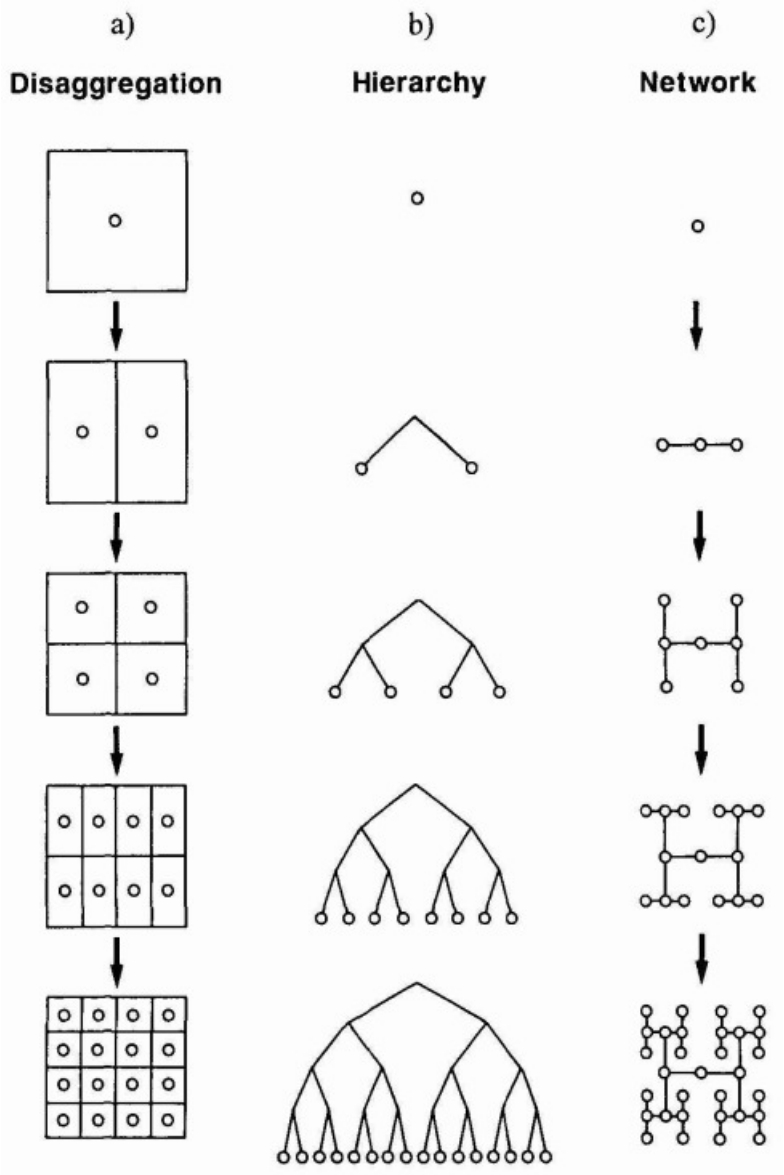

Figure 15: Types of Spatial disaggregation: strict subdivision, hierarchy and network structure (Batty & Longley, 1994).

Fractals consist of self-similar components that form a hierarchy. The tree is a famous example of fractals, which are arranged hierarchically at various sizes. The tree, a literal depiction of hierarchy, symbolizes the most primitive fractal. There are several more instances of hierarchy, including the organization and spacing of cities as centre sites, the arrangement of districts and neighbourhoods, and the geographical distribution of highways and other modes of communication. To describe a few of the clear connections that control binary or dichotomous branching systems we use the formula

$$N_k = v^k \tag{2}$$

where v is the bifurcation ratio and is equal to 2 for binary branching, 3 for ternary branching, and so forth, gives the number of branches of any tree that are formed at a particular level of recursion or hierarchy k. The total of these numbers over k, expressed as

$$N_K = \sum_{1}^{k} N_k \tag{3}$$

determines the number of branches at any level of the hierarchy. The number of elementary operations in every recursive system at any level k could be determined using both equations. Many correlations have been found between branch lengths and widths, angles, scaling or contraction, and symmetry in botanical trees; we will only discuss one of these links, which was initially proposed by Leonardo da Vinci in 16th-century Italy (Batty & Longley, 1994). This is predicated on the idea that the two stems that branch off of any given stem in a tree between levels k - 1 and k are equal in width,

$$W_{k-1}^{s} = {}_{R}W_{k}{}^{s} + {}_{L}W_{k}{}^{s} \tag{4}$$

where W is the branch width, R and L are the right and left branches respectively, and s is a parameter for this relation. When the parameter s is set to 2, as proposed by Leonardo, the tree can be considered Pythagorean since the branch stem width W_{k-1} equals the hypotenuse of a right-angled triangle with sides ${}_{R}W_{k}$ and ${}_{L}W_{k}$. Some propose that W_k, the width of a branch, should be proportional to its length, with

$$W_k \propto L_k^{3/2} \tag{5}$$

The parameter s (here) is unlikely to be as low as 2 but never higher than 3 to make the relationship plausible. The primary factor influencing a tree's shape is its branching angles, but these have no bearing on how we calculate the fractal dimension, which is solely dependent on the number of branches connected to each stem or trunk and the rate at which the branches scale or contract.

3.2 Hofstadter's Butterfly

Hofstadter's butterfly is a self-similar fractal pattern that arises when a crystal lattice is placed in a magnetic field. We will use this as a calculation focused example of a fractal in nature. One of the main reasons that the discovery of this fractal was intriguing is because it involved two well-studied, yet starkly different physical phenomena: electronic band structure and Landau levels (Satija, 2016). Electronic band structure is underpinned by Bloch's theorem, which states that electrons (aptly named Bloch electrons) on a periodic lattice can be described using plane waves. These bands, which describe the possible energy values that these Bloch electrons can take, are continuous. This is not necessarily dismissive of band gaps that can arise in the overall electronic band structure of a crystal since we are concerned with electrons in the conduction band. Landau levels describe the energies that isolated electrons can take while in the presence of a magnetic field. These energy levels are a discrete spectrum of values and have gaps between them. It is from these two energetic phenomena that Hofstadter's butterfly emerges.

3.2.1 Harper's Equation

Obtaining Hofstadter's butterfly involves finding solutions to what is known as Harper's equation. As such, we will begin with a description of what Harper's equation is and how it came to be. We will have to hand-wave some of the technical details which are likely better left to a condensed matter physics course, but we will still encompass the main concepts in its derivation. In short, Harper's equation is Schrödinger's equation for Bloch electrons on a two-dimensional crystal lattice in the presence of a homogeneous magnetic field (Hofstadter, 1976). In order to obtain the necessary form of Schrödinger's equation, we start by utilizing the tight-binding approximation for a square lattice. This simply means that we assume our electrons can only exist at a lattice site (a.k.a. an ion core) and nowhere in between. In doing so, we can write an equation for the Bloch band (or Bloch energy function):

$$E(\mathbf{k}) = 2E_0(cos(ak_x) + cos(ak_y)) \tag{6}$$

where $\mathbf{k}$ denotes the wave vector (k_x, k_y), E_0 is a constant, and a is the lattice spacing.

Now, we must make a substitution for the wave vector such that equation (6) becomes an operator that can act on a wavefunction. This is one of the details that we will gloss over as it is slightly more technically involved, however, the importance of this substitution must be underscored. First carried out by Rudolf Peierls, the substitution to make $E(\mathbf{k})$ into an operator that allows for a form of Schrödinger's equation to be written required, in Douglas Hofstadter's own words, "some true touches of genius" (Satija, 2016). Bypassing the details and proofs, the wave vector $\mathbf{k}$ can be replaced by an electron's canonical momentum in the presence of a magnetic field and using the Landau gauge. This allows us to incorporate the previously missing contribution of the magnetic field through the lattice. Upon substitution and a variety of expansions and approximations, we are left with a Schrodinger's equation that relates the wavefunction of a Bloch electron at a given site to its nearest-neighbours (Hofstadter, 1976):

$$E_0[\psi(x+a,y) + \psi(x-a,y) + e^{\frac{-ieBax}{\hbar c}}\psi(x,y+a) + e^{\frac{ieBax}{\hbar c}}\psi(x,y-a)] = E\psi(x,y). \tag{7}$$

There are a few further simplifications that are made to reach Harper's equation. Firstly, in order to do away with with x and y variables, we can denote each lattice site as an integer multiple of the lattice spacing. This is fairly straightforward since we are working with a square lattice: $x = ma$ and $y = na$. Next, we make the substitutions $\alpha = \frac{a^2Be}{hc}$ and $\epsilon = \frac{E}{E_0}$ (for reasons that will soon be apparent). If we then recognize that our two-dimensional Bloch wavefunctions can be written as $\psi(m,n) = \psi_n\psi_m$, we can finally write Harper's equation:

$$\psi_{m+1} + \psi_{m-1} + 2\cos(2\pi\alpha m - k_y)\psi_m = \epsilon\psi_m. \tag{8}$$

Now, finding the quantities necessary to plot Hofstadter's butterfly has boiled down to an approachable eigenvalue problem. Just as we treat other many-particle Hamiltonians, we can write Harper's equation as a matrix equation (Satija, 2016):

$$\begin{bmatrix} C_1 & 1 & 0 & 0 & 0 & \cdot & e^{-ik_x} \\ 1 & C_2 & 1 & 0 & 0 & \cdot & 0 \\ 0 & 1 & C_3 & 1 & 0 & \cdot & 0 \\ 0 & \cdot & \cdot & \cdot & \cdot & \cdot & 0 \\ \cdot & \cdot & \cdot & \cdot & \cdot & \cdot & \cdot \\ \cdot & \cdot & \cdot & \cdot & \cdot & \cdot & 1 \\ e^{ik_x} & 0 & 0 & 0 & \cdot & 1 & C_q \end{bmatrix} \begin{bmatrix} \psi_1 \\ \psi_2 \\ \psi_3 \\ \cdot \\ \cdot \\ \cdot \\ \psi_q \end{bmatrix} = \epsilon \begin{bmatrix} \psi_1 \\ \psi_2 \\ \psi_3 \\ \cdot \\ \cdot \\ \cdot \\ \psi_q \end{bmatrix}. \tag{9}$$

Here, C_m is the cosine term in our Hamiltonian: $C_m = 2\cos(2\pi\alpha m - k_y)$. Writing Harper's equation in this form now allows us to use the numerical method of exact diagonalization to solve the eigenvalue problem.

3.2.2 Plot of Hofstadter's Butterfly

The fractal pattern occurs when two key quantities are plotted against one another. The first quantity, α, is plotted along the y-axis and is the ratio between the magnetic flux through a unit cell (for a square lattice, a^2B) and a quantum of magnetic flux ($\frac{hc}{e}$). This ratio gives rise to an interestingly dimensionless quantity whose rationality or irrationality dictates the structure of the plot and encodes information about the strength of the magnetic field (Hofstadter, 1976). This quantity can be simplified to $\alpha = \frac{p}{q}$ where p and q are integers and q is related to the periodicity of our lattice. The second quantity, ϵ, is plotted along the x-axis and is related to the energy that electrons can take. It turns out that ϵ is also dimensionless. (The convention for which quantity is plotted on which axis does not generally matter given that the pattern will arise regardless, but this convention is that of Hofstadter's original paper.)

With all of this in mind, plotting Hofstadter's butterfly involves iterating over values of $\alpha = \frac{p}{q}$ in the interval $[0, 1]$ and solving the corresponding exact diagonalization problem for the values of ϵ (Turhan, 2023). Having α bounded in such a way ends up restricting ϵ to $[-4, 4]$ (Hofstadter, 1976). Plots for $q = 5, 50$ are found in figure 16.

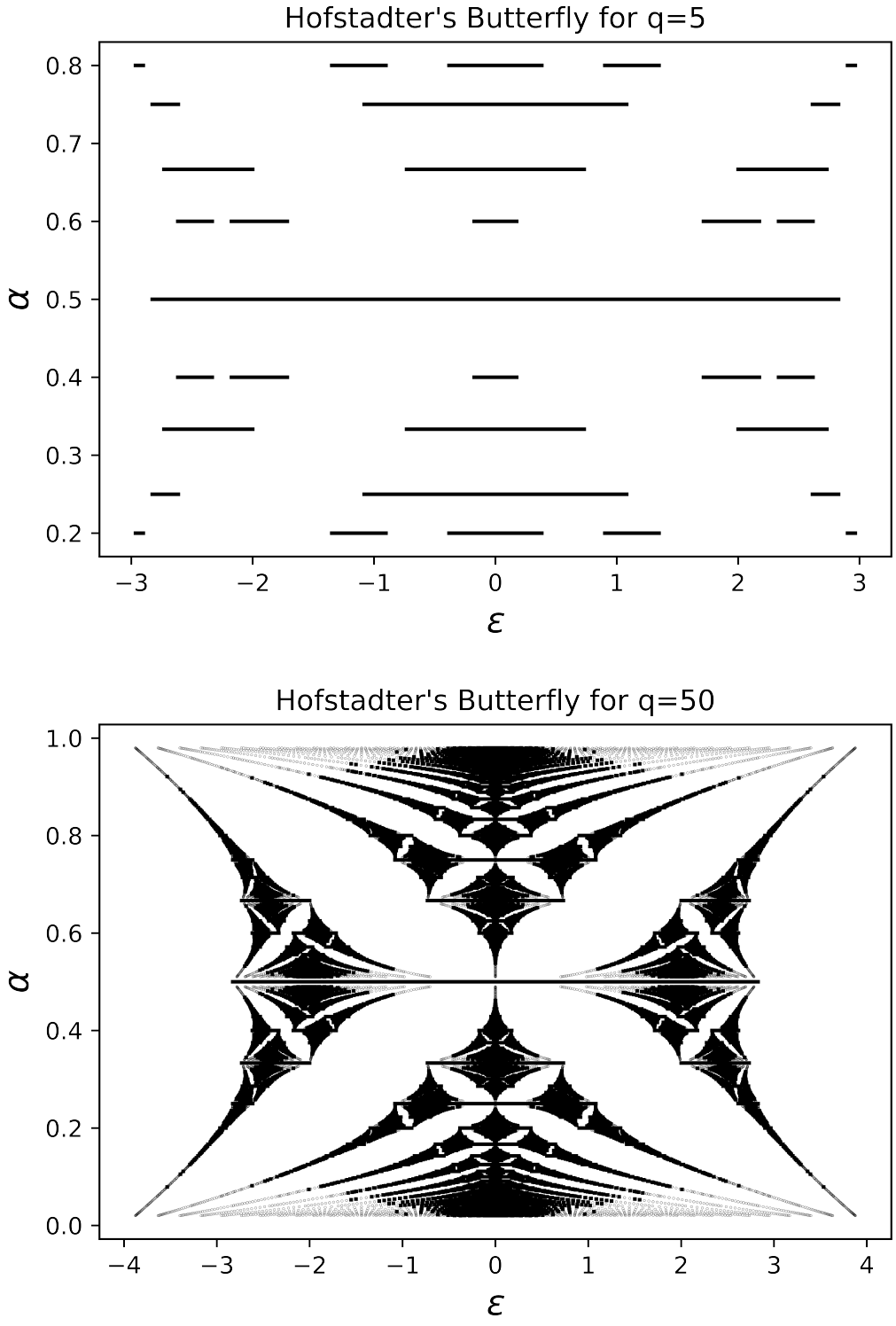

Figure 16: Plots of Hofstadter's butterfly using exact diagonalization method for q=5,50.

The mathematical depth of describing Hofstadter's butterfly through the lens of its recursive structure its quite involved. However, there are a few characteristics that can be pointed out from the original work in Hofstadter, 1976 and subsequent investigation by Ketzmerick et al., 1998. A band corresponding to a value of α can be split into 3 sub-bands: left (L), centre (C), and right (R). The way in which the sub-bands are clustered can be predicted by defining a "local variable" for a value of α, β. We shall present Hofstadter's example with $\alpha = \frac{5}{17}$ to demonstrate how one can determine the clustering of a band. Since the fractal pattern is symmetric, determining β' for L and R will be the same: $\alpha = (N + \beta')^{-1}$. With $N = 3$, $\beta' = \frac{2}{5}$, which means that there will be 5 sub-bands (corresponding to the denominator of β') in L and R. For C, we instead want β' such that $\alpha = [2 + (\beta')^{-1}]^{-1}$. In our case, $\beta' = \frac{5}{7}$, meaning that C will have 7 sub-bands. This same algorithm can be applied again in order to obtain the sub-bands of the sub-bands. Doing so leaves us with an overall band structure (not to be confused with the strict definition of electronic band structure) of $(2-1-2)-(2-3-2)-(2-1-2)$. Visually,:

$$(- -\ -\ - -) \quad (- -\ - - -\ - -) \quad (- -\ -\ - -) \tag{10}$$

where the brackets would of course be omitted in an actual plot of this cluster. According to Hofstadter, determining the number of times one must repeat this algorithm to establish sub-bands is "difficult to predict." However, the case for which α is an irrational value is far more straightforward since these values give rise to the Cantor set. Additionally, irrational α values will correspond to sub-bands that have Hausdorff dimension that is $\leq \frac{1}{2}$ (Ketzmerick et al., 1998).

3.2.3 Closing Remarks on Hofstadter's Butterfly

The sheer breadth of investigation into Hofstadter's butterfly and its related mathematical and physical phenomena is immense. Some of the many areas of study include its relation to number theory, the quantum Hall effect, and extending our knowledge of quasicrystals, which is fairly intractable currently. The fantastic monograph by professor Indubala Satija, *Butterfly in the Quantum World: The story of the most fascinating quantum fractal*, with contributions from Douglas Hofstadter himself alongside a variety of key figures in condensed matter physics and mathematics, compiles many of these topics into one enlightening and entertaining read (Satija, 2016).

4 Conclusion

From the results of analyzing properties of fractals to the application in industry, and from the recognized fractal dimension and patterns to identifying cancer cells, the theories behind fractals have brought upon countless innovations. From small crystallized structures in condensed matter to unintentional fractal growth in the development of cities, the self-similar and hierarchy properties in objects are noticeable everywhere. The interdisciplinary field of fractals continues to shine a light on the chaotic nature of the universe.

References

Barnsley, M. F., & Demko, S. (1985). Iterated function systems and the global construction of fractals. *Proceedings of the Royal Society of London. Series A, Mathematical and Physical Sciences*, *399*(1817), 243–275. Retrieved March 30, 2024, from http://www.jstor.org/stable/2397690

Barnsley, M. F. (1993). *Fractals everywhere (2nd edition)*. Elsevier. https://app.knovel.com/hotlink/toc/id:kpFEE00013/fractals-everywhere-2nd/fractals-everywhere-2nd

Batty, M., & Longley, P. (1994). *Fractal cities: A geometry of form and function*. ACADEMIC PRESS LIMITED.

Commuri, V., Mionis, S., Tan, B., & Wang, W. (2020). *Fast fractal image compression* [Department of Electrical and Computer Engineering, School of Computer Science, Carnegie Mellon University].

Elkington, L., Adhikari, P., & Pradhan, P. (2022). Fractal dimension analysis to detect the progress of cancer using transmission optical microscopy. *Biophysica*. https://doi.org/10.3390/biophysica2010005

Hofstadter, D. R. (1976). Energy levels and wave functions of bloch electrons in rational and irrational magnetic fields. *Physical Review B*, *14*(6), 2239–2249. https://doi.org/10.1103/physrevb.14.2239

Ketzmerick, R., Kruse, K., Steinbach, F., & Geisel, T. (1998). Covering property of hofstadter's butterfly. *Physical Review B*, *58*(15), 9881–9885. https://doi.org/10.1103/physrevb.58.9881

Mazet, V. (2020). *What is a digital image? - basics of image processing*. https://vincmazet.github.io/bip/digital-images/definition.html

Satija, I. I. (2016, August). *Butterfly in the quantum world: The story of the most fascinating quantum fractal*. Morgan Claypool Publishers. https://doi.org/10.1088/978-1-6817-4117-8

Strogatz, S. H. (2015). *Non-linear dynamics and chaos (2nd edition)*. CRC Press.

Turhan, U. C. (2023). *How to plot hofstadter butterflyfractal in python*. https://python.plainenglish.io/how-to-plot-hofstadter-butterfly-fractal-in-python-ddf9846173fc

Welstead, S. T. (1999). *Fractal and wavelet image compression techniques*. SPIE Optical Engineering Press.

Whitney, V. (2018). *Fractal cities*. https://medium.com/data-mining-the-city/fractal-cities-d39e63ce23bb